Journal of Power Sources 191 (2009) 289–296

Contents lists available at ScienceDirect

Journal of Power Sources

journal homepage: www.elsevier.com/locate/jpowsour

Electrochemical characterization of a polybenzimidazole-based high temperature proton exchange membrane unit cell

Jesper Lebæk Jespersen [a,b,*], Erik Schaltz [b], Søren Knudsen Kær [b]

[a] Danish Technological Institute, Kongsvang Allé 29, DK-8000 Aarhus C, Denmark
[b] Aalborg University, Institute of Energy Technology, Pontoppidansstræde 101, DK-9220 Aalborg Ø, Denmark

ARTICLE INFO

Article history:
Received 27 October 2008
Received in revised form 19 January 2009
Accepted 8 February 2009
Available online 20 February 2009

Keywords:
EIS
HT-PEM
Fuel cell
Electrochemical characterization

ABSTRACT

This work constitutes detailed EIS (Electrochemical Impedance Spectroscopy) measurements on a PBI-based HT-PEM unit cell. By means of EIS the fuel cell is characterized in several modes of operation by varying the current density, temperature and the stoichiometry of the reactant gases. Using Equivalent Circuit (EC) modeling key parameters, such as the membrane resistance, charge transfer resistance and gas transfer resistance are identified, however the physical interpretation of the parameters derived from EC's are doubtful as discussed in this paper. The EC model proposed, which is a modified Randles circuit, provides a reasonably good fit at all the conditions tested. The measurements reveal that the cell temperature is an important parameter, which influences the cell performance significantly, especially the charge transfer resistance proved to be very temperature dependent. The transport of oxygen to the Oxygen Reduction Reaction (ORR) likewise has a substantial effect on the impedance spectra, results showed that the gas transfer resistance has an exponential-like dependency on the air stoichiometry. Based on the present results and results found in recent publications it is still not clear what exactly causes the distinctive low frequency loop occurring at oxygen starvation. Contrary to the oxygen transport, the transport of hydrogen to the Hydrogen Oxidation Reaction (HOR), in the stoichiometry range investigated in this study, shows no measurable change in the impedance data. Generally, this work is expected to provide a basis for future development of impedance-based fuel cell diagnostic systems for HT-PEM fuel cell.

1. Introduction

High Temperature Proton Exchange Membrane (HT-PEM) fuel cells based on a polybenzimidazole (PBI) membrane with phosphoric acid as a ionic conductor, first discovered by Wainrigth et al. [1], have shown to have good conductivity at elevated temperatures [2], which gives advantageous features when operated on reformed hydrogen gas [3]. PBI-based HT-PEM can tolerate a high level of impurities in the feed gas, due to the higher operating temperature, where desorption of impurities, such as carbon monoxide, occurs much faster than in low temperature PEM fuel cells. Moreover, the higher operating temperature facilitates better utilization of the waste heat from the fuel cell, e.g. to preheat the fuel or as heat supply for the endothermic steam reforming process of the fuel reformer. A HT-PEM is therefore advantageous to use in conjunction with a fuel reformer when compared to low temperature PEMFC.

As HT-PEM fuel cells are relatively new, detailed experimental characterization of this type of fuel cell is scarce in the literature. Experimental characterization of fuel cells is essential for developers of computational models of fuel cells in order for them to verify and validate their simulation results. Often validation is performed against *I–V* curves, which is insufficient and often misleading [4]. Therefore, data with a high level of detail is needed, and EIS is an excellent tool for providing that. Electrochemical Impedance Spectroscopy (EIS), also known as AC impedance spectroscopy, benefits from being an *in situ* non-intrusive method, which makes it very suitable for detailed characterization and has thus been used to study fuel cells for a relatively long time [5,6]. So far EIS has mainly been used in material research and development, i.e. in the search for new catalyst and membrane materials. Recently, the method has also been extensively used for diagnostics and control of fuel cell systems [7–10], which also means that EIS has been used to study fuel cell stacks [11] as well as single cells. There is a need to develop advanced fuel cell diagnostics systems, in order for fuel cell systems to intelligently adapt the operating conditions to suit the requirements of the system, e.g. long life time or high CO tolerance. Diagnostics also become an important tool for fault detection on fuel cell stacks that do not live up to expected requirements. There is therefore a demand for a flexible

* Corresponding author at: Danish Technological Institute, Kongsvang Allé 29, DK-8000 Aarhus C, Denmark. Tel.: +45 7220 1251; fax: +45 7220 1019.
E-mail address: jesper.jespersen@teknologisk.dk (J.L. Jespersen).
URL: http://www.iet.aau.dk (S.K. Kær).

0378-7753/$ – see front matter © 2009 Elsevier B.V. All rights reserved.
doi:10.1016/j.jpowsour.2009.02.025

and non-intrusive diagnostic system and EIS may be a solution to that.

Especially for HT-PEM fuel cell there is a lack of data, and little work is so far reported on EIS measurements on this type of fuel cell [12]. Jalani et al. used impedance spectroscopy to analyze temperature effects, anode and cathode stoichiometries, oxygen vs. air and the effect of anode humidification on PBI-based H_3PO_4 fuel cells, however only in a narrow range of operating conditions. Lobato et al. investigated the effects of temperature on membrane hydration and catalyst particle agglomeration [13]. Hu et al. recorded the impedance spectra four times over a 500 h continuous test, and found that the main degradation at 640 mA cm^{-2} was caused by agglomeration of platinum particles in the catalyst layers [14]. The same group recently published results of a simulation model, in which AC impedance data, such as internal membrane resistance and apparent area exchange current density, was used [15]. Zhang et al. [16] published their experimental work on a PBI-based MEA measured by EIS in the temperature range of 120–200 °C. Schaltz et al. [17] reported EIS measurements on a single cell HT-PEM for equivalent circuit modeling, and the present work should be considered as an extension of that and providing additional data to the above-mentioned work of EIS on PBI-based HT-PEM fuel cells.

This paper presents detailed (EIS) measurements for various conditions on a single cell HT-PEM. The conditions varied during the measurements are temperature, air stoichiometry, hydrogen stoichiometry and current density. Thus this paper provides detailed information of the effects of changing these conditions, using impedance spectroscopy combined with Equivalent Circuit (EC) modelling (Table 1).

2. Methods

EIS is commonly used in the electrochemical industry to characterize various electrochemical reactions, such as those occurring in batteries [5] and corrosion processes [18]. EIS is also a very common and proven tool within fuel cell research and development to characterize catalyst and membrane materials. EC modeling is used to derive physical parameters from the impedance spectra, i.e. using Nyquist plots.

2.1. Apparatus

A single cell test setup was used in this work similar to one used by Korsgaard et al. [3]. The experimental setup, see Fig. 1, involves a unit cell setup from BASF, a load module, an EIS-software module and a fuel cell control module. The single cell setup constitutes a commercial MEA, which consists of a PBI-membrane (BASF Celtic®-P Series 1000 MEA) with an active area of 45.16 cm^2. A woven carbon cloth, with a thickness of 400 μm was used as gas diffusion layer. Mass flow controllers from Bürkert (air: MFC 8711 0–5 L min^{-1} and hydrogen: MFC 8712 0–1 L min^{-1}) were used to control the flow of reactant gases. The load module used was a TDI Dynaload RBL488 50-150-800 capable of implying sinusoidal fluctuation of the load, both in galvanostatic and potentiostatic mode, in the range of 50 mHz to 20 kHz. The EIS equipment used was the Gamry FC350 Fuel Cell Monitor, which is compatible with the TDI load module.

Table 1
List of symbols.

λ_{air}	Stoichiometric ratio of air	[−]
λ_{H_2}	Stoichiometric ratio of hydrogen	[−]
R_m	Membrane resistance	[Ω]
R_c	Contact resistance	[Ω]
R_s	Resistance of cell components	[Ω]
$Z_{gt,W}$	Impedance of gas transfer	[Ω]
$R_{W,gt}$	Finite length warburg resistance	[Ω]
T_W	Diffusion interpretation parameter	[−]
j	Square root of −1	[−]
ω	Angular frequency	[rad/s]
p	Finite length coefficient	[−]
$R_{gt,tot}$	Gas transfer resistance	[Ω]
R_{gt}	Low frequency loop resistance	[Ω]

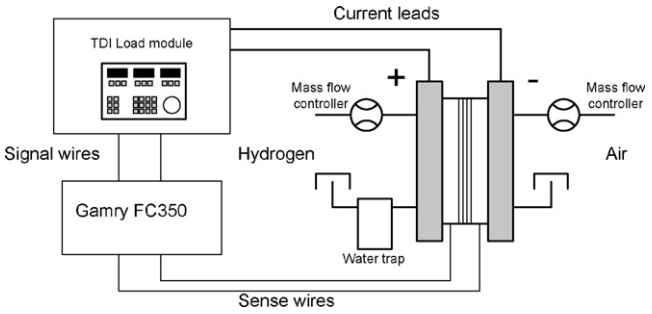

Fig. 1. Layout of test setup.

The EIS experiments conducted were controlled by the Fuel Cell Monitor FC-350 from Gamry. The flow of reactants and control of temperature was carried out through a Labview environment. During an EIS measurement the stoichiometry of the reactant gases was kept constant in accordance with the selected DC current.

2.2. Experimental procedure

In order to prepare the MEA for optimal performance some actions were taken according to the manufacturer's instructions. Initially, the MEA was prebaked at 140 °C for 2 h, in order to remove potential water vapor from the porous structures of the MEA. Afterwards, the MEA was installed in the single cell test setup and clamping bolts were tightened with a torque screwdriver to ensure an even pressure distribution to the MEA. The MEA was hereafter subject to a break-in procedure (MEA conditioning), which involved running at 0.2 A cm^{-2}(≈9 A) at 160 °C for 100 h, with stoichiometry ratios of $\lambda_{air} = 2.5$ and $\lambda_{H_2} = 2.5$. Hereafter, a polarization (I–V) curve was recorded, with a current gradient of 30 s/A, shown in Fig. 2.

In order to ensure a rational execution of the experiments a test scheme was prepared, as seen in Table 2. In total, 42 impedance

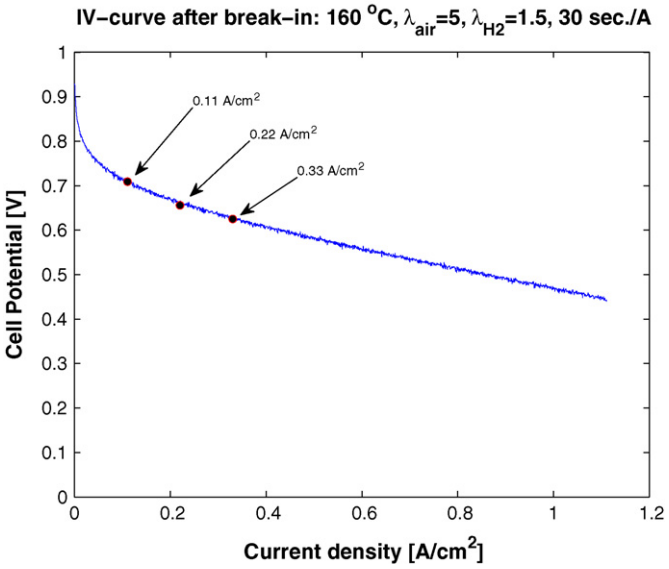

Fig. 2. I–V curve after 100 h break-in.

Table 2
Test scheme for EIS measurements in chronological order.

Exp. ID#	Current density [A cm^{-2}]	Temperature [°C]	λ_{air}	λ_{H_2}
1	0.11	110	5	1.5
2	0.22	110	5	1.5
3	0.33	110	5	1.5
4	0.11	120	5	1.5
5	0.22	120	5	1.5
6	0.33	120	5	1.5
7	0.11	130	5	1.5
8	0.22	130	5	1.5
9	0.33	130	5	1.5
10	0.11	140	5	1.5
11	0.22	140	5	1.5
12	0.33	140	5	1.5
13	0.11	150	5	1.5
14	0.22	150	5	1.5
15	0.33	150	5	1.5
16	0.11	160	5	1.5
17	0.22	160	5	1.5
18	0.33	160	5	1.5
19	0.33	160	10	1.5
20	0.33	160	8	1.5
21	0.33	160	5	1.5
22	0.33	160	4	1.5
23	0.33	160	3	1.5
24	0.33	160	2	1.5
25	0.33	160	1.5	1.5
26	0.33	160	1.2	1.5
27	0.33	160	1.1	1.5
28	0.33	160	5	4
29	0.33	160	5	3
30	0.33	160	5	2
31	0.33	160	5	1.5
32	0.33	160	5	1.2
33	0.33	160	5	1.1
34	0.11	170	5	1.5
35	0.22	170	5	1.5
36	0.33	170	5	1.5
37	0.11	180	5	1.5
38	0.22	180	5	1.5
39	0.33	180	5	1.5
40	0.11	190	5	1.5
41	0.22	190	5	1.5
42	0.33	190	5	1.5

spectra were recorded. The tests are arranged in chronological order and each EIS spectrum is labeled with an experimental ID ("ID#"), this labeling is used in Section 3. The test scheme was arranged so that low temperature measurements were conducted initially in order to avoid degradation at high temperatures [13,19,20]. At each temperature three impedance spectra were recorded at the different current densities indicated in Fig. 2. Tests for investigating the effects of changing the gas stoichiometry were conducted at 160 °C as this is considered to be the nominal operating temperature for this type of fuel cell running on pure hydrogen. All tests were galvanostatic measurements carried out in "hybrid" mode [21] using a current amplitude resulting in an AC voltage of 2.5 mV rms.

2.3. Experimental artifacts

No impedance system is perfect and experimental artifacts are induced by several factors. Some of them can be eliminated and others are hardware related and cannot be changed. Good practice for experimental impedance studies can be found in the literature [5,10,22]. In this study experimental artifacts were minimized by: using shielded sense wires, polishing the terminals of the current leads, using as short as possible current leads and the use of twisted wires for the control signal to the load module. Fig. 3 shows a typical EIS plot for this type of fuel cell. One measurement error that is present in all datasets is the inductive behavior occurring at high frequencies (10–20 kHz). Generally, this error can be related to the leads of the cell [23,22,24]. Leads with a length of 1 m were used in this experiment, it was not possible to further shorten the leads, due to the physical constraints of the test setup. Choosing the appropriate band of the load bank can also influence the measurements, see Section 3.1 for more information on this issue.

The low frequency inductive loop, which occurs at frequencies ¡ 1 Hz, could have several explanations and is currently discussed in the literature. Roy and co-workers [25] list a number of reasons to this phenomenon, however models and measurements from their work indicated that it is associated with the formation of hydrogen peroxide at the ORR.

2.4. Equivalent circuit modeling

In order to provide a better insight and evaluation of the changes in the impedance spectra, Equivalent Circuit (EC) modeling, also named transmission line equivalent circuit [26], is a useful tool. Using electric components, such as resistors and capacitors, the impedance spectrum can be simulated in the entire frequency range. The challenge is however to provide a model that gives a sufficiently good fit at every frequency point, that is physically sound and a model that can adapt to changes in the operating conditions. Observations of the experimental data is therefore needed in order to provide a sound physical model of the system [27]. The quality of a fit can be evaluated using the χ^2-value, however the data and the model should also be subject to a visual examination.

The physical interpretation of the EC is important in order to understand the physical changes occurring in the system. An easy interpretation of the EC is to divide the losses in the MEA into an anodic loss, a membrane loss and a cathodic loss in which the losses associated with mass transport limitations are included. An informative schematic representation of the Nyquist plot using that interpretation can be found in the literature [11,28,29]. Although, this representation is informative and easily understood, it may not be an accurate description. The loop occurring in the high frequency region, called the anodic loss, and the loop in the low frequency region, called the cathodic loss cannot be separated in such a way. Occurrences on the anode side can influence the cathodic loss region, as it is the case for CO poisoning [30]. Moreover, Yuan et. al [31] showed results where the anode was starved, this did not affect the high frequency loop, but had a significant effect on the low frequency loop. It is therefore better to distinguish between the high frequency loop and the low frequency loop in order to avoid conflicts with the physical understanding of the system.

Zhang et al. [16] proposed a modified Randles cell equivalent circuit for a PBI-based HT-PEM fuel cell, the equivalent circuit modeling of this paper is based on this model. In Fig. 4 an equivalent circuit model for a PBI-based HT-PEM fuel cell is proposed. The components of the unit cell and MEA can be coupled to the three parts

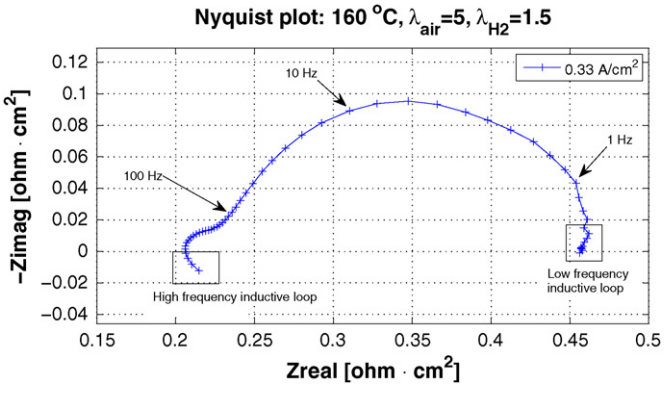

Fig. 3. Typical Nyquist plot of PBI-based fuel cell impedance spectra.

of the EC circuit, as shown in the figure. The full lines represent the most important contributions to the loss, while the dotted lines represent minor contributions. Even though this may be a better physical representation of the system, the losses in the three parts of the EC cannot be considered independent of each other, however general tendencies can be derived and can be considered valid. Below the parts of the EC model are explained.

2.4.1. Ohmic resistance

The Ohmic resistance is often referred to as the solution resistance in corrosion science and is the combined ohmic resistance of several components of the cell assembly. In a regular *I–V* curve the ohmic resistance resembles the linear part of the curve. The main contribution to this term is the electrolyte resistance or membrane resistance, the Ohmic resistance is therefore often referred to as the membrane resistance, R_m. The membrane resistance, R_m can be divided into the contact resistance, R_c, and the Ohmic resistance of the cell components, R_s, as described in [32,11]:

$$R_m = R_c + R_s \quad (1)$$

The contact resistance, but also the resistance of the cell components, is dependent on the clamping pressure of the cell fixture as recently showed by Chang et al. [33]. It is therefore important to ensure that the clamping pressure is kept constant during all measurements. In this experiment the seals of the test rig ensures that a correct clamping pressure is achieved, as the PTFE seals (Nowoflon PFA 370 μm) used can be considered as incompressible. Hence, the eight bolts of the test rig were tightened with a small torque wrench, ensuring that the MEA reached a compression that reassembles the thickness of the seals. These eight bolts were fitted with disc springs, to compensate for the thermal expansion of the cell. Other factors influencing the ohmic resistance are humidification, when considering the low temperature PFSA-type membranes [7,8,11] and temperature in the form of drying or evaporation of the proton conducting media [13].

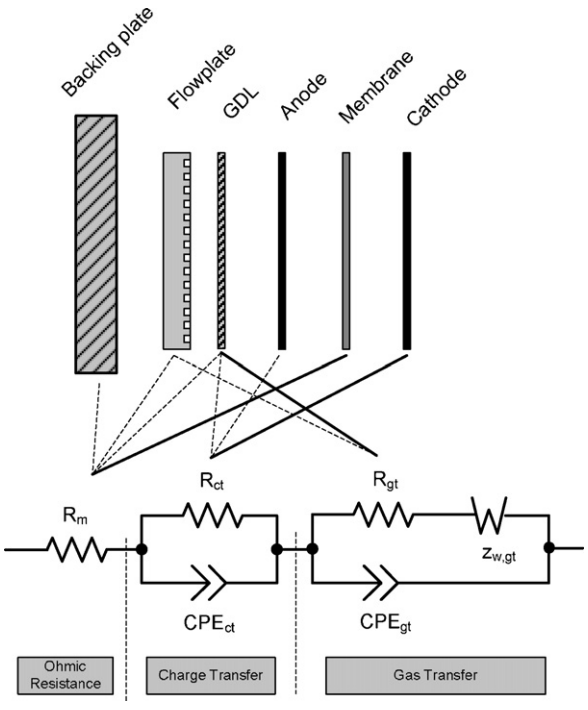

Fig. 4. Equivalent circuit for an HT-PEM fuel cell.

2.4.2. Charge transfer

The resistance associated with transfer of charge, R_{ct}, mainly stems from the Oxygen Reduction Reaction (ORR), as indicated in Fig. 4, which is mainly due to the slow reaction of reducing oxygen. Minor contributions are the Hydrogen Oxidation Reaction (HOR) and capacitive charge storage in the porous structure of the GDL and electrodes. This part of the model is associated with the high frequency section of the spectrum.

2.4.3. Gas transfer

The gas transfer resistance is associated with transfer of reactant gasses to the active sites of the electrodes. This is mainly governed by mass transfer on the cathode side in terms of convection in the channels of the bipolar plate and diffusion in the GDL and electrodes. As hydrogen by nature is much more diffusive and generally has better transport capabilities than oxygen, the anode side only has minor contributions to this loss. The gas transfer resistance is associated with the low frequency part of the spectrum. In order to account for diffusion a finite length warburg element was added to the EC circuit shown in Fig. 4. The finite length warburg element is defined as:

$$Z_{gt,W} = R_{W,gt}\frac{\tanh((T_W j\omega)^p)}{(T_W j\omega)^p} \quad (2)$$

In order to enable finite length diffusion, which is the case for a fuel cell, the coefficient p is set to $p = 0.5$. $R_{W,gt}$ is the finite length warburg gas transfer resistance, T_W is the diffusion interpretation parameter, which defines the frequency response [18]. The total gas transfer resistance $R_{gt,tot}$ is a combination of the low frequency loop resistance R_{gt} and the finite length warburg resistance $R_{W,gt}$ and is defined as:

$$R_{gt,tot} = R_{gt} + R_{W,gt} \quad (3)$$

3. Results and discussion

The results of the experimental investigation are divided into the following four subcategories:

- Current density
- Temperature
- Air stoichiometry
- Hydrogen stoichiometry

The impedance spectra are analyzed by means of EC modeling in relation to the above parameters in order to provide a more clear understanding of the transport and electrochemical processes occurring at the interfaces of the MEA under investigation.

3.1. Current density

The DC current drawn from the cell during impedance spectroscopy has a huge impact on the recorded spectrum. The capacitative charge in the porous structure of the Gas Diffusion Electrode (GDE) and the Gas Diffusion Layer (GDL) is striped for electrons faster at high current densities, which is illustrated in Fig. 5 where the capacitive loops are larger at low current densities. At low current densities the cell is limited by kinetics of the reactions, similar results were found in the literature [25,22]. This is also illustrated in Fig. 2, where 0.11 A cm^{-2} is in the region of the *I–V* curve dominated by activation losses. It is therefore also essential that data is recorded at the same DC current if direct comparison is made. Noise can be created due to the operation modes of the electronic load, which has three different current range settings: high (150 A), medium (20 A) and low (2 A), all measurements in this study were performed in the medium range. This can have

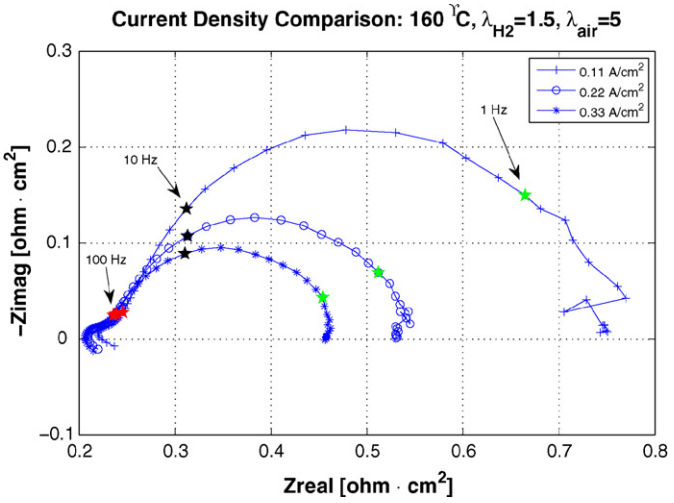

Fig. 5. Nyquist plot showing the impedance spectra at different current densities.

a significant impact on the noise level in the readings, when operating in the lower end of the range scale, e.g. at a current density of 0.11 A cm^{-2}, corresponding to a DC current of 5 A, because of the lower resolution of the current output signal. It is clear to see how the accuracy of the data increases, when observing Fig. 5 as one moves to higher current densities, especially at low frequencies (¡ 1 Hz).

3.2. Temperature

The operating temperature for a PBI HT-PEM fuel cell is an extremely important parameter. In order to operate the cell, the membrane temperature must exceed 100 °C, as water is on vapor form and will therefore not absorb the excess phosphoric acid 'free acid' that is not bound directly to the PBI matrix and transport it out of the cell. This 'free acid' is reported to contribute significantly to the membrane proton conductivity [2]. Too high cell temperatures, will however enhance degradation, in terms of increased hydration of the electrolyte [13,19], increased agglomoration/sintering of the platinum catalyst particles [13] and carbon corrosion of the catalyst support [20]. The optimal operating temperature of a PBI fuel cell therefore depends on the requirements of the application in which it will be used. Hence, if a long life time is needed, a low cell temperature is preferred, or if high CO tolerance is needed, high cell temperature is preferred [3].

3.2.1. Membrane resistance

The proton conductivity is strongly dependent on temperature [34,35,19] and it is commonly known that elevated temperatures increase the rate of an electrochemical reaction. Thus, changing the operating temperature of a fuel cell must give rise to changes in the impedance spectrum. The impedance spectrum was recorded for temperatures ranging from 110 to 190 °C with an interval of 10 K, see Table 2. The current densities during these measurements were 0.11, 0.22 and 0.33 A cm^{-2} at stoichiometric ratios of $\lambda_{H_2} = 1.5$ and $\lambda_{air} = 5$. Fig. 6 shows the impedance spectra recorded at the 9 different temperatures at 0.33 A cm^{-2}. From the figure it is clear that the kinetics of the ORR are improved at elevated temperatures as the LF loop is minimized at higher temperatures, this is cosistent with other findings in the litterature [36,15,12]. Also the membrane resistance, indicated by the high frequency intercept where Zimag = 0 in Fig. 6, is displaying a slight shift to the left in the Nyquist plot.

The electrochemical software 'Zview' was used to perform fitting of the EC model, seen in Fig. 4. The data from the model is presented in Figs. 7 and 8. Zview outputs an error percentage for each of the

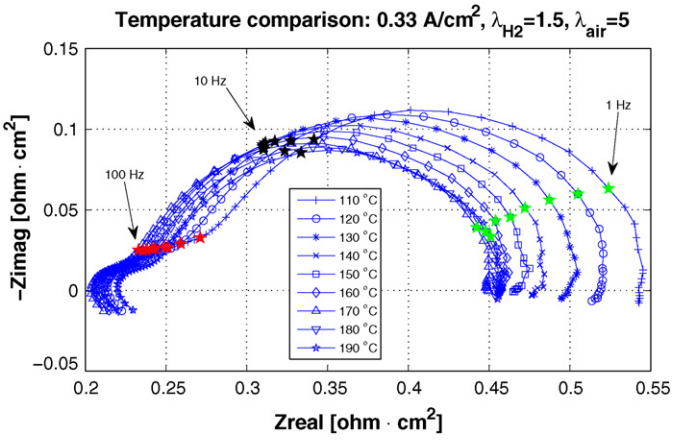

Fig. 6. Nyquist plot showing the impedance spectra at different temperatures using a current density of 0.33 A cm^{-2}.

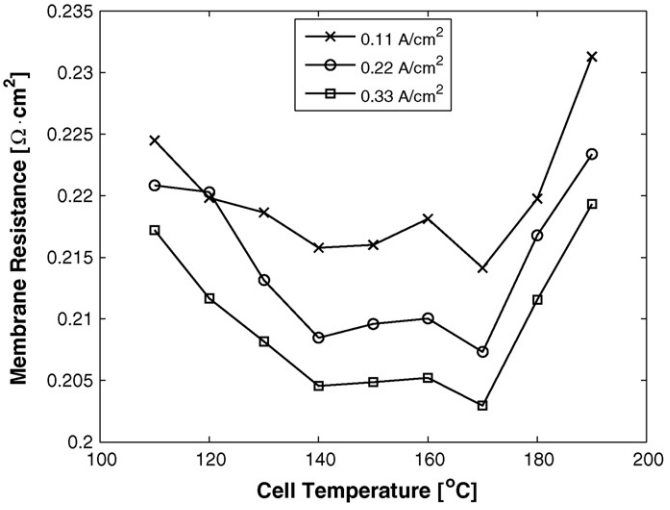

Fig. 7. Membrane resistance as a function of temperature and current density.

elements in the EC model, all the data presented in Fig. 7 and 8 had an error percentage lower than 8%.

When analyzing the fit results from the EC model, as shown in Fig. 7 the membrane resistance is gradually decreasing until

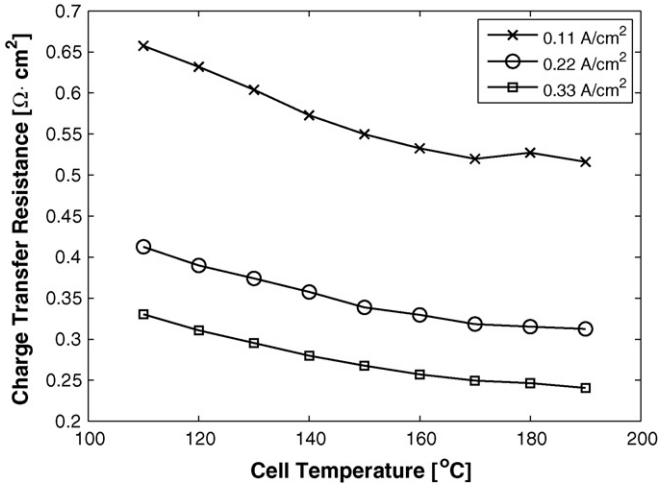

Fig. 8. Charge transfer resistances as a function of cell temperature and current density.

140 °C, where it levels out until 170 °C where an increase is observed beyond the level at low temperatures. These results are not consistent with the results reported by Zhang et al. [16], Hu et al. [15] and Ma et al. [19], it is unclear what causes these significant deviations at high temperatures (180–190 °C) from the data found in the literature. The data is however not easy to compare; Zhang et al. only provides two data points, which makes a thorough comparison difficult. When observing the path of the spectrum, the impedance spectra recorded by Hu et al. differs from what was found in this work and by others, as only one capacitive loop is present, whereas most other studies using PBI-based MEA have two conjoined loops [37,16,13]. The reason for this difference could be explained by the home-made MEA used by Hu et al. They do however report a lower membrane resistance when the temperature is increased. At 120 °C the data points for 0.11 and 0.22 A cm^{-2} seems to intersect, this is believed to stem from noise in the measurements and especially uncertainties from the EC fitting procedure. These noise and uncertainty issues may be solved by repeating the experiment and perform averaging of the results.

When observing the membrane resistance as a function of current density, is seen that the membrane resistance is lowered when current density is increased, and this tendency applies for the entire temperature range. This is in good coherence with the findings of Zhang et al. [16] who observed a slight drop in membrane resistance from 0 to 1 A cm^{-2}, whereas at high current densities the membrane resistance remains constant. Zhang et al. explains this as a balance between the water produced and the water removed by the reactants, which becomes stable at high current densities ¿ 1 A cm^{-2}.

3.2.2. Charge transfer resistance

The EC model described in Section 2.4 includes gas transfer resistance as a part of the model. However, when the cell is supplied with a sufficient flow of reactants the gas transfer resistance becomes negligible or at least constant if the flow remains unchanged. When gas transfer resistance is included in the EC model and the cell is supplied with sufficient reactants the gas transfer part of the EC model should be added to the charge transfer part of the model. The gas transfer part is added to model the second semicircle which arises from low stoichiometric conditions. Therefore the gas transfer part will act as part of the charge transfer part of the model when operating at sufficient stoichiometric conditions, when the second semicircle is not present. Fig. 8 shows the combined charge transfer resistance. The charge transfer resistance is strongly related to the current density, this is also evident in Fig. 5 and also supported by the measurements made by Zhang et al. [16]. The effect of temperature on the charge transfer resistance is not very significant, this applies for all the current densities investigated. The temperature does however have a small effect on the kinetics, which also coherent with the data from Zhang et al. and Hu et al. [15], although is not as apparent a change as in the data provided by Hu et al. The reason for the temperature dependency on the charge transfer is that the reaction kinetics at the anode (HOR) and the cathode (ORR) are temperature dependent, such as any other electrochemical reaction. At low current densities, such as this case, the charge transfer resistance is mainly governed by the ORR [16].

3.2.3. Gas transfer resistance

As mentioned above the gas transfer resistance in the temperature data set is not investigated as the cell was operated with sufficiently high stoichiometric ratios on both the anode and cathode, so that the gas transfer resistance remains unaffected and is therefore neglected. If the temperature effect on the gas transfer resistance where to be investigated measurements should be made with lower stoichiometric conditions. There are no such data present at the moment, Jalani et al. [37] did however report measurements in a similar current density range, but with pure oxygen as oxidant. The gas transfer resistance is also reported to be very current density-dependent at higher current densities (1–2 A cm^2) [16].

3.3. Air stoichiometry

The structure of the GDL and gas channels are important in relation to the gas transfer resistance, they can be described as follows: the MEA used was a Celtec P-1000 from BASF, which features a woven carbon cloth as GDL, the cathode gas channels where three parallel serpentine shaped with a width of 1.2 mm and a depth of 1 mm, the anode gas channels where two parallel serpentine shaped with a width of 1.2 mm and a depth of 1 mm. The width of the land area for both flow plates where 1.2 mm.

The effects of changing the stoichiometric ratios of the feed gasses were investigated at a constant temperature of $t_{cell} = 160$ °C and a current density of 0.33 A cm^{-2}. Normally, mass transport limitations to fuel cell performance occurs at high current densities (¡ 1 A cm^{-2}), in this study a relatively low current density (0.33 A cm^{-2}) was used and instead the air supply was varied by means of the air stoichiometry. This should reveal some of the same phenomenon as at high current densities, as the concentration in the gas channels and the GDL also will change as a function of air stoichiometry. Naturally, this does not provide the same information as a full investigation including high current densities, but that is beyond the scope of this paper. Both the cathode and anode stoichiometries were investigated. Springer and Wilson [38] showed that the oxygen electrode is very sensitive to the oxygen concentration. Therefore changing the air stoichiometry has a dramatic effect on the Oxygen Reduction Reaction (ORR) and hence the impedance spectra, as can be seen in Fig. 9. An additional semicircle is formed at low frequencies (¿ 1 Hz), when the cell is subject to mass transport limitations at the cathode electrode. This is in coherence with the work published by Ciureanu and Roberge [32]. At low stoichiometric conditions the cell displays very poor dynamic capabilities, the cell is simply starved at the cathode. In Fig. 10 the gas transfer resistance is plotted as a function of air stoichiometry. From the figure it can be seen that air stoichiometries above four ($\lambda_{air} > 4$) have little or no effect on the cell performance. Therefore there is no reason to operate the cell at higher stoichiometries from an electrochemical point of view; there could however be other reasons why air stoichiometries $\lambda_{air} > 4$ are interesting, such as cooling.

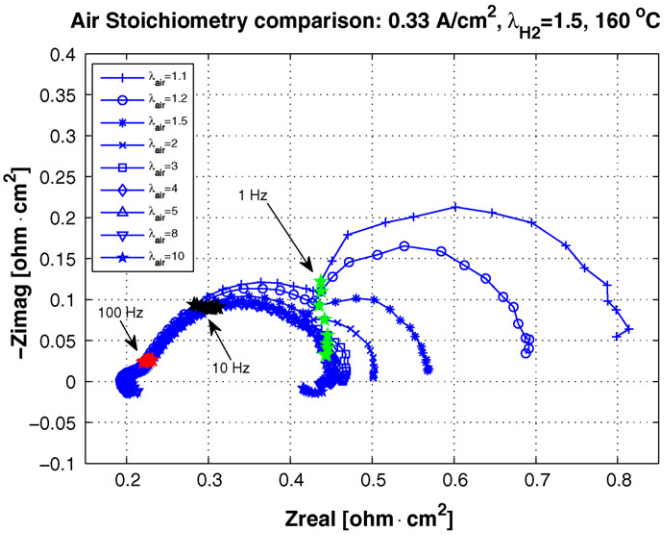

Fig. 9. Nyquist plot showing the impedance spectra at different air stoichiometries.

The impedance response during oxygen depletion has previously been reported in numerous papers [39,32,31,37,40–43,16]. Ciureanu and Roberge [32] investigated the LF loop in a Nafion-based PEM fuel cell at low temperatures and low currents, where flooding becomes important. In their study they assign the LF loop to be generated from air limitation to the backing/catalyst layer interface caused by the accumulation of liquid water in the pores of the backing layer.

Results have shown that impedance measurements are a global in-plane measurement method and the in-plane variations can be significant [41]. Recent localized measurements performed by Schneider et al. [42,43] contradict the theory of the thin film agglomerate model [32,39] as data indicate that the low frequency loop stems from over-potentials in the downstream parts of the flow channel caused by oscillations of the oxygen partial pressure generated upstream in the flow channel. This supports the measurements shown in Fig. 9 as no liquid water is present in the micro-porous layers of the MEA of an HT-PEM fuel cell, no diffusion limitation cased by a thin film of water in the porous structure of the MEA can therefore occur. Results from impedance measurements on fuel cells with different flow fields [36] also contradicts the thin film agglomerate theory as interdigitated flow fields seems to eliminate the low frequency semi-circle. In an interdigitated flow field the flow is forced through the GDL by convection, oscillations in the channels will therefore be suppressed as the pressure drop is much higher than conventional flow fields. However, the LF frequency loop is most likely governed by both the length of the channel, as Schneider et al. theory suggest, and it is dependent on the GDL structure.

It is believed by the authors of this paper that more experimental work has to be carried out in this field in order to fully understand this phenomenon and thereby build a supporting model that can simulate the AC response of low stoichiometric conditions on the cathode side, using a sound physical understanding. The authors suggest that experiments with different flow fields (serpentine, interdigitated) and different GDL structures (thickness, structure) are carried out on an HT-PEM fuel cell to avoid a thin film of water.

3.4. Hydrogen stoichiometry

When operating on ambient air the rate limiting reaction is the ORR. Therefore, changing the hydrogen stoichiometry has little effect on the HOR and thus on the overall performance of the fuel cell. This is illustrated in Fig. 11. As can be seen from the figure

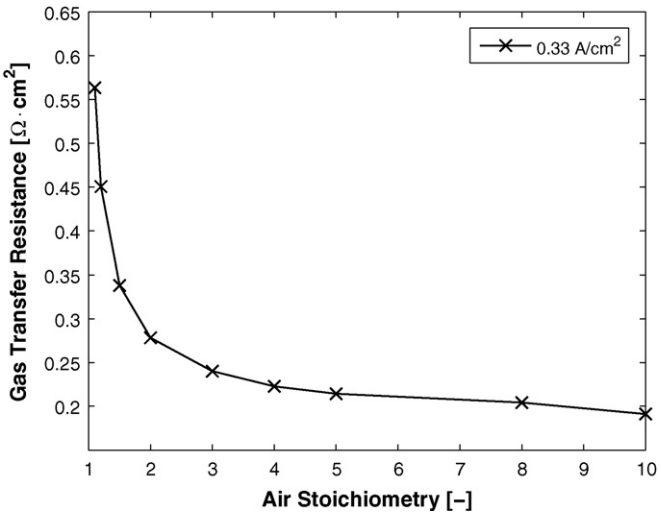

Fig. 10. Gas Transfer Resistance as a function of air stoichiometry.

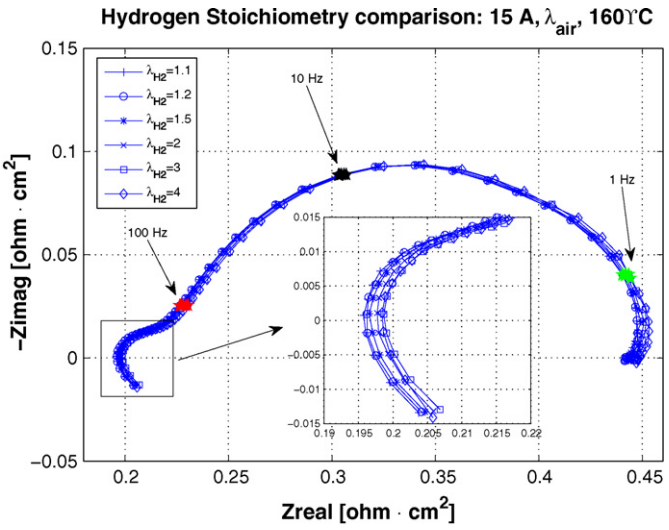

Fig. 11. Nyquist plot showing the impedance spectra at different hydrogen stoichiometries.

the impedance spectra are almost identical at all stoichiometries, only a slight change in the membrane resistance is observed. The consistency in the data is due to the diffusive nature of hydrogen, the molecules can easily diffuse through the GDL and reach the active sites of the anode catalyst and dissociate into electrons and hydrogen protons.

The amount of AC impedance studies investigating hydrogen stoichiometry is very scarce. Jalani et al. [37] showed that if the hydrogen stoichiometry is unity ($\lambda_{H_2} = 1$) then a pure diffusion-limited trend takes place identified by a 45 °C straight line. It is assumed that the impedance spectra shown in Fig. 11 will take a similar trend when subject to ($\lambda_{H_2} = 1$).

No secondary low frequency loop was detected on the anode side as it was the case on the cathode side, see Fig. 9. This agrees with the theory proposed by Schneider et al. [42,43] as no concentration oscillations can occur on the anode side as only hydrogen is present there. Moreover, the diffusive nature of hydrogen allows for better mass transport to the anode electrode. Hence, no low frequency loop appears on the anode side.

4. Conclusion

A polybenzimidazole high temperature unit cell was analyzed in various modes of operation using AC impedance spectroscopy, with the main purpose of providing a data set for future impedance-based fuel cell diagnostic systems. EC modeling was used to derive physically related parameters from the fuel cell, a modified Randles cell was used for this purpose. The model was able to provide a reasonably good fit of the experimental data in all modes of operation in the study, which proves that a generic and flexible model is found. From the model and the experimental data it was found that the temperature has some influence on the ohmic resistance, i.e. membrane resistance, which is also a function of current. The charge transfer resistance, which is a measure of the reaction kinetics, showed a strong dependence on temperature, whereas current is less important. The gas transfer resistance, which is a measure of the mass transport limitations to the reactive sites, showed a strong dependence on current and a somewhat weaker dependence on temperature.

The cell was also tested for the effect of changing the stoichiometry of the inlet gases. The impedance spectra provides a very clear and distinct signal when the cell is fed with a low air stoichiometry; however the exact nature of why this low frequency semicircle

appears is still being discussed in the literature. Based on the data in this study and published results it is concluded that the semicircle is a function of both the GDL structure and the gas channel structure; however, more experiments are needed in order to fully understand this phenomenon. Results in the present study showed that the cell should be operated at $\lambda_{air} > 4$ in order to avoid significant losses due to mass transport of oxygen. Results from investigating the effect of hydrogen stoichiometry showed that low hydrogen stoichiometry only has a marginal influence on the impedance spectra.

Acknowledgements

This work was partly sponsored by the Danish Technological Institute and The Danish Ministry of Science, Technology and Innovation, within the Industrial PhD-programme.

References

[1] J. Wainright, J.-T. Wang, D. Weng, R. Savinell, M. Litt, J. Electrochem. Soc. 142 (1995) 121–123.
[2] Q. Li, R. He, R.W. Berg, H.A. Hjuler, N.J. Bjerrum, Solid State Ionics 168 (1–2) (2004) 177–185.
[3] A.R. Korsgaard, R. Refshauge, M.P. Nielsen, M. Bang, S.K. Kaer, J. Power Sources 162 (1) (2006) 239–245.
[4] C.Y. Wang, Chem. Rev. 104 (10) (2004) 4727–4765.
[5] E. Barsoukov, J.R. Macdonald, Impedance Spectroscopy: Theory, Experiment, and Applications, Palo Alto, CA, 2006.
[6] T.E. Springer, T.A. Zawodzinski, M.S. Wilson, S. Gottesfeld, J. Electrochem. Soc. 143 (2) (1996) 587–599.
[7] J.-M.L. Canut, R.M. Abouatallah, D.A. Harrington, J. Electrochem. Soc. 153 (5) (2006) A857–A864.
[8] N. Fouquet, C. Doulet, C. Nouillant, G. Dauphin-Tanguy, B. Ould-Bouamama, J. Power Sources 159 (2) (2006) 905–913.
[9] T. Kurz, A. Hakenjos, J. Krämer, M. Zedda, C. Agert, J. Power Sources 180 (2) (2008) 742–747.
[10] W. Merida, D. Harrington, J. Le Canut, G. McLean, J. Power Sources 161 (1) (2006) 264–274.
[11] W.H. Zhu, R.U. Payne, B.J. Tatarchuk, J. Power Sources 168 (1) (2007) 211–217.
[12] J. Zhang, Z. Xie, J. Zhang, Y. Tang, C. Songa, T. Navessin, Z. Shi, D. Songa, H. Wang, D.P. Wilkinson, Z.-S. Liu, S. Holdcroft, J. Power Sources 160 (2006) 872–891.
[13] J. Lobato, P. Canizares, M.A. Rodrigo, J.J. Linares, Electrochim. Acta 52 (12) (2007) 3910–3920.
[14] J. Hu, H. Zhang, Y. Zhai, G. Liu, J. Hu, B. Yi, Electrochim. Acta 52 (2) (2006) 394–401.
[15] J. Hu, H. Zhang, L. Gang, Energy Convers. Manage. 49 (5) (2008) 1019–1027.
[16] J. Zhang, Y. Tang, C. Song, J. Zhang, J. Power Sources 172 (1) (2007) 163–171.
[17] E. Schaltz, J.L. Jespersen, P.O. Rasmussen, 2006 Fuel Cell Seminar, Honolulu, Hawaii, 2006.
[18] R. Cottis, S. Turgoose, Corrosion Testing Made Easy: Electrochemical Impedance and Noise, NACE, 1993.
[19] Y.-L. Ma, J.S. Wainright, M.H. Litt, R.F. Savinell, J. Electrochem. Soc. 151 (1) (2004) A8–A16.
[20] T.J. Schmidt, J. Baurmeister, J. Power Sources 176 (2) (2008) 428–434.
[21] G. Instruments, Gamry FC-350 Operation Manual.
[22] M.F.M. Rohit Makharia, D.R. Baker, J. Electrochem. Soc. 152 (5) (2005) A970–A977.
[23] S.K. Roy, M.E. Orazem, J. Electrochem. Soc. 154 (8) (2007) B883–B891.
[24] A. Hombrados, L. González, M. Rubio, W. Agila, E. Villanueva, D. Guinea, E. Chinarro, B. Moreno, J. Jurado, J. Power Sources 151 (2005) 25–31.
[25] M.E.O. Sunil, K. Roy, B. Tribollet, J. Electrochem. Soc. 154 (12) (2007) B1378–B1388.
[26] M. Eikerling, A.A. Kornyshev, J. Electroanal. Chem. 475 (2) (1999) 107–123.
[27] M.E. Orazem, B. Tribollet, Electrochim. Acta 53 (2008) 7360–7366.
[28] R. O'Hayre, S.-W. Cha, W. Colella, F. Prinz, Fuel Cell Fundamentals, John Wiley & Sons, 2006.
[29] R. O'Hayre, S.-W. Cha, W. Colella, F.B. Prinz, Fuel Cell Fundamentals, John Wiley & Sons, Inc., 2006.
[30] R.C. Jiang, H.R. Kunz, J.M. Fenton, J. Electrochem. Soc. 152 (7) (2005) A1329–A1340.
[31] X. Yuan, J.C. Sun, M. Blanco, H. Wang, J. Zhang, D.P. Wilkinson, J. Power Sources 161 (2) (2006) 920–928.
[32] M. Ciureanu, R. Roberge, J. Phys. Chem. B 105 (17) (2001) 3531–3539.
[33] W. Chang, J. Hwang, F. Weng, S. Chan, J. Power Sources 166 (1) (2007) 149–154.
[34] J. Lobato, P. Cañizares, M. Rodrigo, J. Linares, G. Manjavacas, J. Membr. Sci. 280 (1–2) (2006) 351–362.
[35] L. Qingfeng, H. Hjuler, N. Bjerrum, J. Appl. Electrochem. 31 (7) (2001) 773–779.
[36] S.-S. H. Sheng-Huang Yang, C. Lun Feng, Proceedings of FUELCELL2006, The 4th International Conference on Fuel Cell Science, Engineering and Technology, 2006.
[37] N.H. Jalani, M. Ramani, K. Ohlsson, S. Buelte, G. Pacifico, R. Pollard, R. Staudt, R. Datta, J. Power Sources 160 (2) (2006) 1096–1103.
[38] S.G.T.E. Springer, M.S. Wilson, J. Electrochem. Soc. 140 (1993) 3513–3526.
[39] Y. Bultel, K. Wiezell, F. Jaouen, P. Ozil, G. Lindbergh, Electrochim. Acta 51 (3) (2005) 474–488.
[40] D. Gerteisen, A. Hakenjos, J.O. Schumacher, J. Power Sources 173 (1) (2007) 346–356.
[41] I.A. Schneider, H. Kuhn, A. Wokaun, G.G. Scherer, J. Electrochem. Soc. 152 (10) (2005) A2092–A2103.
[42] I.A. Schneider, S.A. Freunberger, D. Kramer, A. Wokaun, G.G. Scherer, J. Electrochem. Soc. 154 (4) (2007) B383–B388.
[43] I.A. Schneider, D. Kramer, A. Wokaun, G.G. Scherer, J. Electrochem. Soc. 154 (8) (2007) B770–B782.